Synthesis and Characterization of a β-Hairpin Peptide That Represents a 'Core Module' of Bovine Pancreatic Trypsin Inhibitor (BPTI)[†,‡]

Natalia Carulla,[§] Clare Woodward,[||] and George Barany*[,§]

Department of Chemistry, University of Minnesota, Minneapolis, Minnesota 55455, and Department of Biochemistry, Molecular Biology, and Biophysics, University of Minnesota, St. Paul, Minnesota 55108

Received December 22, 1999; Revised Manuscript Received April 17, 2000

ABSTRACT: A new strategy for the design and construction of peptide fragments that can achieve defined, nativelike secondary structure is presented. The strategy is based upon the hypothesis that 'core elements' of a protein, synthesized in a single polypeptide molecule, will favor nativelike structure, and that by incorporating a cross-link, nativelike core structure will dominate the ensemble as the more extended conformations are excluded. 'Core elements' are the elements of packed secondary structure that contain the slowest exchanging backbone amide protons in the native protein. The 'core elements' in bovine pancreatic trypsin inhibitor (BPTI) are the two long strands of antiparallel β-sheet (residues 18−24 and 29−35) and the small β-bridge (residues 43−44). To test the design strategy, we synthesized an 'oxidized core module', which contains the antiparallel strands connected by a modified reverse turn (A27 replaced by D), a natural disulfide cross-link at the open end of the hairpin, and *N*- and *C*-termini blocking groups. A peptide with identical sequence but lacking the disulfide cross-link at the open end was used as the 'reduced core module' control. The conformational behavior of both peptides was examined using ^{1}H NMR spectroscopy. Chemical shift dispersion, chemical shift deviation from random coil values, sequential and long-range NOEs, and H/D amide exchange rates were compared for the two peptides. We conclude that the ensemble of oxidized and reduced core module conformations samples both nativelike 4:4 and non-native 3:5 β-hairpin structure, and that the oxidized module samples nativelike structure for a greater fraction of the time than the reduced module.

Identification of protein submolecular domains that can exist as autonomous units favoring nativelike structure would find numerous applications in protein design, as an aid to the production of peptides whose favored structure is predictable. From the crystal structure, it is difficult to recognize which protein sequences may constitute folding subdomains, because in many regards all buried regions of a protein are similar: interior atoms are well packed, hydrogen bond donors/acceptors are matched with complementary protein sites or with buried waters, and secondary structure elements make good supersecondary contacts. We aim to develop new strategies for identification and construction of folding subdomains based on a dynamic property of the protein, amide hydrogen exchange (*1*). Protein 'core elements', stretches of residues containing the slowest exchanging NH protons in the native protein, tend to have the most stable nonlocal interactions whether the protein is unfolded (*2*), partially folded (*3*, *4*), or fully folded. Our hypothesis is that we can identify the core motif of a protein from hydrogen exchange data, and then design and construct a single polypeptide molecule, or 'core module', composed of core elements, which favor nativelike structure.

To test this strategy, we focus on the protein bovine pancreatic trypsin inhibitor (BPTI),[1] for which the core elements are two long strands of antiparallel β-sheet (18−24, 29−35) (Figure 1a) and a small β-bridge (43−44). An oxidized core module, containing the antiparallel strands connected by a modified reverse turn (A27 replaced by D27), a natural disulfide cross-link at the open end of the hairpin, and *N*- and *C*-termini blocking groups, was designed and constructed (Figure 1b). A peptide with identical sequence but lacking the disulfide cross-link at the open end is a reduced core module control (Figure 1c). ^{1}H NMR spectroscopic analysis and other techniques show that the ensemble of oxidized and reduced core module conformations favors nativelike β-hairpin structure and that, consistent with the design concepts, oxidized core module samples nativelike

[†] This work was supported by NIH Grant GM 51628 (G.B. and C.W.). N.C. is the recipient of a Louise T. Dosdall Fellowship from the Graduate School of the University of Minnesota.

[‡] Portions of this work were reported in preliminary form (*60*).

* To whom correspondence should be addressed at the Department of Chemistry, University of Minnesota, 207 Pleasant St. S.E., Minneapolis, MN 55455. Phone: 612-625-1028. Fax: 612-626-7541. Email: barany@tc.umn.edu.

[§] Department of Chemistry, University of Minnesota, Minneapolis.

[||] Department of Biochemistry, Molecular Biology, and Biophysics, University of Minnesota, St. Paul.

[1] Abbreviations: Abu or X, α-amino-*n*-butyric acid; BPTI, bovine pancreatic trypsin inhibitor; CD, circular dichroism; DSS, sodium 2,2-dimethyl-2-silapentane-5-sulfonate; DTT, dithiothreitol; ESMS, electrospray mass spectrometry; Fmoc, 9-fluorenylmethoxycarbonyl; FPLC, fast protein liquid chromatography; HPLC, high-performance liquid chromatography; Mpa or B, β-mercaptopropionic acid; NMR, nuclear magnetic resonance; NOESY, nuclear Overhauser effect spectroscopy; SEC, size-exclusion chromatography; TFA, trifluoroacetic acid; TOCSY, total correlation spectroscopy; TSP, sodium 3-trimethylsilylpropionate-*2,2,3,3-d*$_4$.

10.1021/bi992927l CCC: $19.00
Published on Web 06/14/2000

β-hairpin structure for a greater fraction of the time than reduced.

Model systems for folding of β-sheets are particularly challenging because of the tendency to intermolecular aggregation. A number of relatively short peptides (9−16 residues in length) apparently populate two-stranded antiparallel β-sheet (β-hairpin) conformations (*5, 6*). These peptides are made by two different strategies: (i) de novo design (*7*−*14*), and (ii) reproduction of β-hairpin sequences found within naturally folded proteins (*15*−*21*). An example of the latter is the protein GB1, which has two β-hairpins, one of which in isolation forms a monomeric nativelike structure in water (*17*), while the other shows only a small amount of turnlike structure (*16*). We offer an explanation for why protein fragments are sometimes nativelike and sometimes are not: if the peptide consists of hydrogen exchange 'core elements', it is more likely to favor native structure.

MATERIALS AND METHODS

Peptide Synthesis and Purification. The core module linear sequence was assembled by automated Fmoc solid-phase synthesis and cleaved using protocols reported previously from our laboratories (*22*). To minimize racemization, Fmoc-Cys(Trt)-OPfp was used when coupling Cys (*23*). The crude linear reduced core module peptide was analyzed by analytical HPLC using a Vydac C_{18} reversed-phase column (0.46 × 25 cm), and a linear gradient of 0.1% TFA in CH_3CN and 0.1% aqueous TFA was run at a 1.2 mL/min flow rate, started isocratic at 1:3 for 5 min, and then increased to 1:1 over 30 min (t_R 17 min).

The crude reduced core module peptide (50 mg, 17.5 μmol) was oxidized with DMSO (8 mL) in 0.01 M phosphate buffer, pH 7.5 (65 mL), for 24 h at 25 °C. The reaction mixture was lyophilized, and the crude oxidized peptide (t_R 11 min) was analyzed by HPLC under conditions identical to those described for the reduced analogue. All peptides were purified on an FPLC System (Pharmacia) with a HR 16/10 reversed-phase column using a linear gradient of 0.1% TFA in CH_3CN and 0.1% aqueous TFA. Peptide purities were confirmed by analytical HPLC, and identities were confirmed by amino acid analysis and by ESMS; for oxidized core module, calcd: 2854.3, found: *m*/*z* 2853.7 $[MH]^+$; for reduced core module, calcd: 2856.7, found: *m*/*z* 2856.3 $[MH]^+$; and for oxidized module with alanine at position 27 (synthesized, oxidized, and purified the same way), calcd: 2810.5, found: *m*/*z* 2810.1 $[MH]^+$.

Size-Exclusion Chromatography. A Superdex Peptide HR 10/30 column was used in an FPLC System (Pharmacia). Injections of 20 μL were eluted with 50 mM sodium acetate buffer at pH 4.5. Polypeptides of M_r 12 500 (cytochrome *c*), 6500 (BPTI), 2126 (gastrin I), and 1665 (α-MSH) known to exhibit monomeric behavior were used as standards. The oxidized and reduced peptides elute at 16.9 and 14.6 mL, respectively. The peaks were sharp, symmetrical, and without shoulders.

CD Spectroscopy. CD spectra were measured on a JASCO 710 spectropolarimeter equipped with temperature control cells. Spectra were acquired in 100 mM NaCl, 10 mM phosphate buffer at pH 6, at a peptide concentration of 0.16 mM for oxidized core module and 0.09 mM for reduced core module.

NMR Spectroscopy. NMR samples for oxidized core module were 0.5−0.8 mM in 50 mM sodium acetate buffer, pH 4.5, and for reduced core module were 0.5 mM in 5 mM sodium acetate buffer, pH 4.5. For solubility reasons, oxidized samples had higher salt than reduced samples; the latter also contained 20-fold excess DTT. The lyophilized pure peptides were dissolved in water at pH 3, dialyzed (MW cutoff 500) against water without added salt, and adjusted to pH 4.5. Deuterated sodium acetate, pH 4.1, was then added. Samples in D_2O were dialyzed at pH 4.5, lyophilized, and dissolved (done inside a glovebag) in sodium acetate, at pH 4.1 in 99.9% D_2O. Two-dimensional ^1H NMR spectra of oxidized and reduced core modules were obtained in 90: 10 H_2O/D_2O and 99.9% D_2O at 3, 6, 15, 25, 35, and 45 °C on a Varian 600 or 800 MHz Inova instrument. Proton chemical shifts were measured from an internal TSP or DSS standard defined as 0 ppm. Phase-sensitive two-dimensional TOCSY (*24*) and NOESY (*25*) spectra were recorded by standard techniques using the time-proportional phase incrementation mode. Suppression of intense solvent resonances was achieved by presaturation or use of the WATERGATE sequence (*26*). Relatively long mixing times were generally used (τ_m = 400 ms) in NOESY experiments (Figure 6) to allow buildup of medium- and long-range NOEs, although spectra with shorter mixing times (τ_m = 200 ms) were also recorded to avoid misinterpretation as a result of spin diffusion. TOCSY spectra were recorded using a 45 ms MLEV 17 spin-lock sequence. Typically, 64 scans were taken with 2K complex data points in the t_2 dimension and 256 complex FIDs in the t_1 dimension. Data were processed and analyzed using the programs NMRPipe (*27*) and NMRView (*28*). Data points were weighted using either a 45° or a 75° shifted square sine bell in each dimension, and zero filled to form 4K × 2K real matrixes. Baseline corrections were applied in both dimensions. Hydrogen isotope exchange rates were obtained by measuring peak volumes versus times in a series of two-dimensional TOCSY spectra at pH 4.15 and 6 °C for the oxidized core module and at pH 4.4 and 6 °C for the reduced core module. Pseudo-first-order rate constants were determined from nonlinear least-squares fit of an exponential rate equation to experimental data.

Structure Calculations. A Silicon Graphics Octane workstation was used to run the program X-Plor (*29*). Cross-peak volumes in NOESY spectra of oxidized core module in H_2O and D_2O were evaluated qualitatively as strong, medium, and weak and assigned upper limit distance constraints of 3, 4, and 5 Å, respectively. Pseudoatom corrections were added where necessary. Because of conformational averaging in peptides (*30*−*33*), the use of intraresidue and sequential NOEs can complicate the calculation of singular structures existing within the ensemble; therefore, only medium- and long-range NOEs were used. Phi angles were constrained, to the range 0° to −180°, except for Gly (*8, 9, 11, 12*). When only the non-native NOE data set was used, the phi angle for Asp was not constrained since this position in the turn of a 3:5 β-hairpin favors a positive phi angle. Three calculations were performed for oxidized core module: one with the complete set of NOEs (27 medium- and 62 long-range), a second with nativelike NOEs (15 medium- and 36 long-range), and a third with non-native NOEs (12 medium- and 26 long-range). Hydrogen bonds and dihedral angles

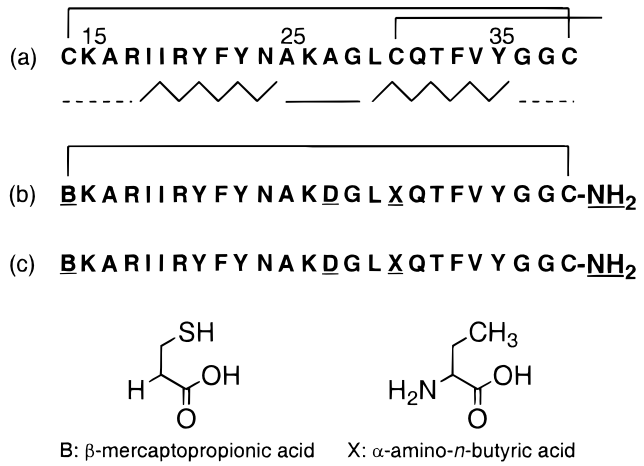

FIGURE 1: Design of the BPTI core modules. Sequences for (a) core template, (b) oxidized core module, and (c) reduced core module. Underlines show differences from the native sequence. The structures of the unnatural amino acids B, β-mercaptopropionic acid, and X, α-amino-*n*-butyric acid, are drawn at the bottom.

were analyzed using the programs HBPLUS (*34*) and PROCHECK (*35*), respectively.

RESULTS AND DISCUSSION

Oxidized and Reduced Core Modules. The oxidized core module of BPTI (Figure 1b) is comprised of 25 residues spanning positions 14−38 of the natural protein, and we retain this numbering in describing both molecules. The peptide contains residues that correspond to both β-sheet strands (18−24 and 29−35) and the critical reverse turn (25−28). To better mimic the native protein, neutral end groups are incorporated; e.g., residue 14 is *N*-terminal β-mercaptopropionate (B in Figure 1), and residue 38 is *C*-terminal cysteinamide. C30 is replaced by α-amino-*n*-butyric acid (X in Figure 1), a substitution which is essentially isosteric and avoids formation of undesired intra- and intermolecular disulfide bonds. The oxidized core module retains the natural 14−38 disulfide cross-link, while the reduced core module does not. A cross-link is added to eliminate from the ensemble of conformations sampled by the peptide those that are more stable because they are highly flexible (have high entropy); the expectation is that among the accessible conformations that remain, nativelike forms will be favored (*36*, *37*). As described under Materials and Methods, peptides of this size and sequence are readily accessed following stepwise chain assembly by Fmoc chemistry; the required oxidation is achieved by treatment with DMSO.

The final design feature was to modify the reverse turn by replacement of the alanine at position 27 by an aspartic acid, based on the assumption that such a change would help to stabilize a type I β-turn (*38*). Both the A27 and D27 peptides are adequately soluble for NMR studies at 0.8 mM. The one-dimensional NH region and the fingerprint region of a TOCSY spectrum are compared for the peptide with A27 and the peptide with D27 in Figures 12 and 13, respectively, in the Supporting Information. Most of the NH backbone resonances for the Ala peptide are overlapped at around 8.5 ppm, whereas the peptide with Asp that is the main focus of the present report has more dispersion of NH backbone resonances, indicating that it favors a population of more structured conformers.

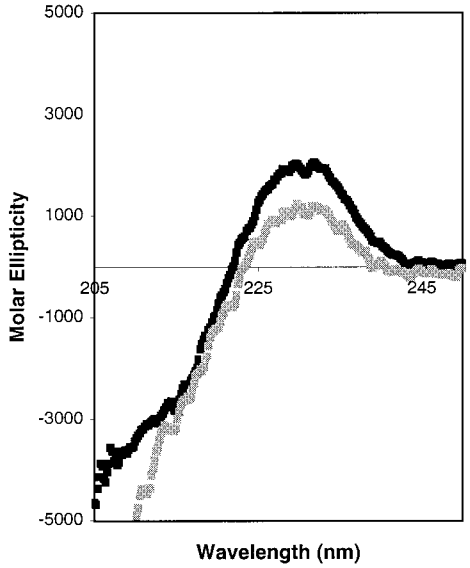

FIGURE 2: CD spectra of oxidized core module (0.16 mM) (black squares) and reduced core module (0.09 mM) (gray squares) at 3 °C in a 100 mM NaCl, 10 mM phosphate buffer at pH 6.

The purified reduced and oxidized peptides, both with the A27D substitution, were examined by size-exclusion chromatography to verify that aggregation does not occur, and to obtain information about their molecular shapes. The peptides behave as monomers under the same pH and salt concentration used for NMR studies (vide infra). The concentration of oxidized core module sample (1.4 mM) for chromatographic analysis was about double that for NMR (0.5−0.8 mM), while the concentration of reduced core module (0.4 mM) was the same as for NMR. The reduced core module elutes earlier than oxidized, indicating that the latter has a smaller hydrodynamic volume, and is, as expected, on average more collapsed than reduced.

In far-UV CD spectra for oxidized and reduced core modules, the signal is relatively weak, and the major feature is the positive band at 230 nm (Figure 2), attributed to the Tyr L_a transition (*39*). We conclude that the CD signals arise from transitions of aromatic residues, and do not represent bands characteristic of assignable secondary structure.[2]

NMR: Assignments and Chemical Shifts. Sequence-specific resonance assignments were determined from NOESY and TOCSY spectra acquired at pH 4.5 in ^1H_2O and ^2H_2O with variable temperature and mixing time (*44*). Tables of complete backbone and side-chain assignments for both peptides are available as Supporting Information. The oxidized core module peptide has considerably more chemical shift dispersion than expected for a random coil, and somewhat more dispersion than found in the reduced core module (Figure 3). Several NH and CαH resonances in the oxidized module are shifted downfield by as much as 0.3 ppm, relative to reduced.

[2] As a companion to their studies of peptides designed to mimic protein folding intermediates (*40*−*42*), Kim and co-workers also constructed a peptide spanning residues 14−38 and including a disulfide bridge (*43*). However, their molecule differs from our oxidized core module by (i) having ionizable end groups, (ii) replacing C30 by a serine residue, and (iii) not modifying the turn. Kim et al. concluded, on the basis of CD spectra similar to those we report in Figure 2, that their model peptide lacked secondary and tertiary structure.

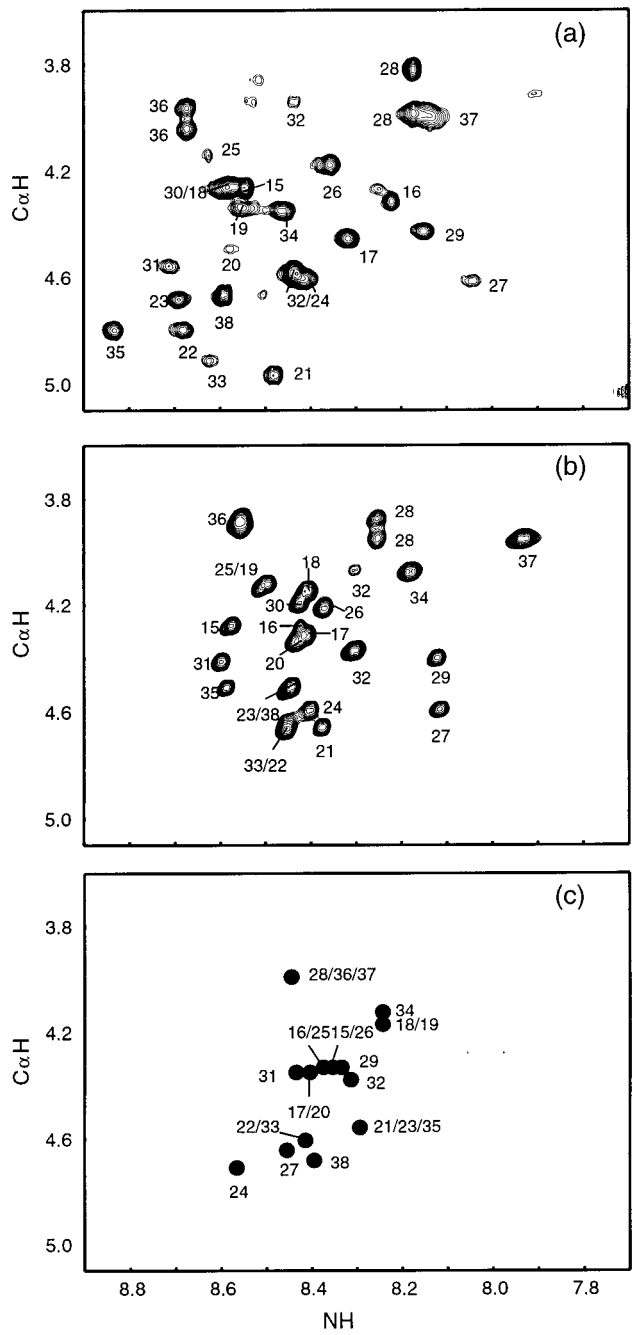

FIGURE 3: The NH−CαH region of the TOCSY spectrum taken at 600 MHz is shown for (a) oxidized core module and (b) reduced core module in $^1H_2O/^2H_2O$ (9:1 by volume) at 3 °C and pH 4.5. Frame c is a plot of random coil NH−CαH chemical shifts (*47, 48*) of amino acids in the core modules, at 3 °C.

CαH chemical shifts in peptides (*30*−*33*) are valuable tools for detection of α-helices (*45, 46*), and β-hairpins (*8, 11, 19, 21*). The deviation of CαH chemical shifts from random coil values predominantly reflects phi/psi values for that residue. Relative to random coil values (*47, 48*), upfield shifts of CαH protons are observed for residues within helix and turn structures, whereas downfield shifts are observed for residues within β-sheet conformations (*49*). The overall pattern of CαH chemical shift deviation from random coil is similar for the module peptides, naturally occurring BPTI, and $[14-38]_{Abu}$ (Figure 4). $[14-38]_{Abu}$ is a partially folded variant of BPTI with nativelike structure in the β-strands. For residues 25−28, which in native BPTI are a turn, the

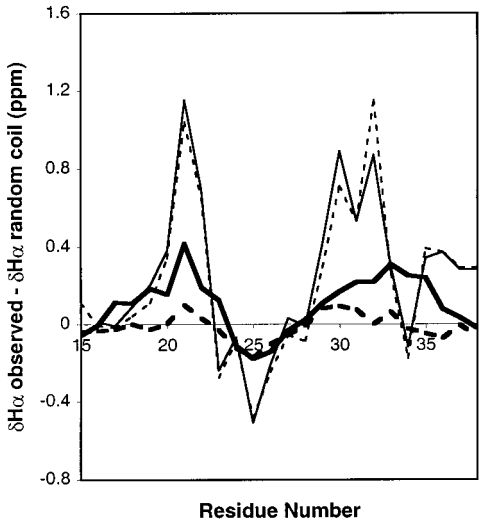

FIGURE 4: Plot of the conformational shifts of CαH protons for oxidized core module (thick solid line), reduced core module (thick dashed line), $[14-38]_{Abu}$ (thin solid line), and native BPTI (thin dashed line).

deviation is negative (upfield shift); for residues 18−24, 29−35, which in native BPTI are strands, it is positive (downfield shift). The magnitude of deviations for residues 25−28 is approximately the same for both peptides (Figure 4). For residues I19, R20, Y21, F22, Q31, T32, F33, V34, and Y35, in the oxidized core module, deviations are 0.2−0.45 ppm, while for the same residues in the reduced core module, deviations are 0.0−0.1 ppm. Oxidized core module has CαH chemical shift deviations similar to native BPTI (*50*) and to $[14-38]_{Abu}$ (*3*) both in the strands and in the turn; this provides an indication that its backbone samples nativelike structure. Reduced core module has some similarity of CαH chemical shift deviations to native BPTI and to $[14-38]_{Abu}$, although to a more significant degree for turn residues than for strand residues.

Sequential Nuclear Overhauser Effects. Sequential backbone NOEs of residues 18−24 and 29−35 in both oxidized and reduced peptides indicate conformational averaging, reflected in the presence of $d_{\alpha N}(i,i+1)$ as well as $d_{NN}(i,i+1)$ NOEs. In both peptides, the intensity ratios $I_{\alpha N}(i,i+1)/I_{NN}(i,i+1)$ are smaller in residues 25−28 than in residues 18−24 and 29−35, suggesting that turnlike conformations are more favored in 25−28 and extended conformations are more favored in 18−24 and 29−35 (Figure 5 and Table 1). The observation of sequential NOEs reporting multiple conformations is well-known (*30*−*33*), for example, in a designed dodecapeptide (*8*) that adopts 30% β-hairpin structure in water.

The Oxidized Core Module Favors a Major Population of 4:4 β-Hairpins in Equilibrium with a Minor Population of 3:5 β-Hairpin.[3] Multiple long-range NOEs are observed

[3] According to Sibanda and Thornton (*51, 52*), β-hairpins are classified as hairpins *X*:*Y* according to the following: *X* and *Y* are the number of residues in the loop, and *X* equals *Y* when the distal strand residues form two backbone hydrogen bonds, whereas $Y = X + 2$ if they form only one. The β-hairpin shown in Figure 7a is a β-hairpin 4:4 because it contains four residues in the loop region, and the distal strand residues, N24 and L29, have two hydrogen bonds, while the β-hairpin shown in Figure 7b is a β-hairpin 3:5 because it has three residues in the loop region and the distal strand residues, N24 and G28, have only one hydrogen bond.

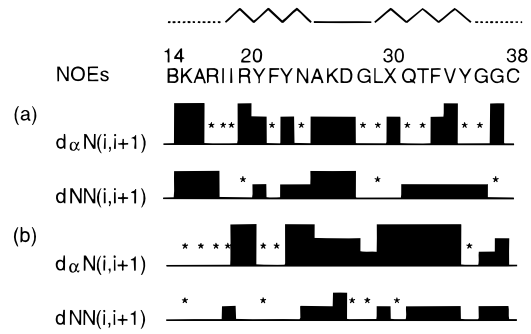

FIGURE 5: Summary of NOE sequential connectivities observed in aqueous solution at 3 °C and pH 4.5 for (a) oxidized core module and (b) reduced core module. The height of each line reflects the intensity of the sequential NOE connectivity, e.g., weak, medium, and strong. An asterisk indicates unobserved NOE connectivity due to signal overlapping or proximity to diagonal. Backbone−backbone NOEs are available in tabulated form in the Supporting Information.

Table 1: Ratios of $I_{\alpha N(i,i+1)}/I_{NN(i,i+1)}$ for Oxidized Core Module and Reduced Core Module[a]

residue *i*	$I_{\alpha N(i,i+1)}/I_{NN(i,i+1)}$ OxCM	$I_{\alpha N(i,i+1)}/I_{NN(i,i+1)}$ RedCM
Tyr 21	3.4	OL[b]
Tyr 23	3.9	NC[c]
Ala 25	1.9	2.1
Lys 26	0.8	1.3
Asp 27	2.3	OL
Leu 29	OL	5.3
Gln 31	OL	6.9
Thr 32	OL	6.5
Phe 33	5.6	6.8
Val 34	7.3	9.6

[a] Residues that correspond to the turn in native BPTI are 25−28. [b] OL indicates that the ratio could not be calculated due to signal overlap or proximity to diagonal. This is indicated as an asterisk in Figure 5. [c] NC indicates that the ratio could not be calculated due to the absence of a cross-peak for NN(*i*,*i*+1).

for the oxidized core module (Figure 6a,c). Due to the averaging inherent in spectra of a conformational ensemble, these NOEs report subpopulations of preferred structures. In contrast, NOEs for native proteins arise from a dominant population of closely related conformations. Several lines of evidence lead us to conclude that the oxidized core module is an equilibrium ensemble of conformations among which a major population is similar to the nativelike 4:4 β-hairpin and a minor population approximates 3:5 β-hairpins. (i) Nativelike backbone CαH−CαH NOEs are about twice as intense as non-native. Likewise, for side-chain−side-chain NOEs, the nativelike are more numerous and more intense than non-native. (ii) Simulated annealing calculations do not support a single family of structures but are consistent with an equilibrium between major 4:4 β-hairpin and minor 3:5 β-hairpin populations. (iii) An equilibrium between 4:4 and 3:5 β-hairpins has also been reported for other peptides (*9*, *11*, *12*). In the three paragraphs that follow, we elaborate on each of these points separately.

First, in native BPTI, turn residues 25−28 and strand residues 18−24 and 29−35 adopt a 4:4 β-hairpin conformation, the structure of which is shown in Figure 7a. All nativelike NOEs in the oxidized module are diagrammed as colored arrows in Figure 7a. These include weak cross-strand NH−NH NOEs between I18−Y35 and R20−F33, and weak and medium cross-strand CαH−CαH NOEs between R17−G36, Y21−T32, and Y23−X30 (Figure 7a and Figure 6c). Other nativelike cross-strand interactions are expected between the NH−NH of F22−Q31 and N24−L29 and between the CαH−CαH of I19−V34, but are too close to the diagonal to be observed in these spectra. In addition to native backbone NOEs in the oxidized module, there are native side-chain−side-chain NOEs between Y21−X30, Y21−T32, Y23−A25, and Y23−X30, and, to a smaller extent, F33−F22 and Y35−I18 (Figure 7a and Figure 6a). While long-range NOEs clearly indicate that the conformational ensemble samples nativelike structure a significant fraction of the time, a number of non-native NOEs indicate a smaller population of non-native 3:5 hairpin conformations. All non-native NOEs in the oxidized module are diagrammed as colored arrows in the 3:5 β-hairpin in Figure 7b. Several are long-range and cross-strand. Since salient characteristics of β-hairpin conformations include CαH−CαH NOEs between interior face-to-face residues (*5*, *6*, *53*, *54*), observation of weak cross-strand, non-native CαH−CαH NOEs between Y23−L29, F33−I19, and Y35−R17 (Figure 6c) is diagnostic of a minor population of 3:5 β-hairpin (Figure 7b). Also consistent with this conclusion, non-native, side-chain−side-chain NOEs between cross-strand residues are between Y23−L29, Y21−Q31, and I19−F33.

Second, simulated annealing calculations have been carried out incorporating all NOEs, but such calculations reveal several obvious distance constraint violations leading us to conclude that no single population of conformers explains all the observed NOEs. The most frequent violations are between CαH protons in interior face-to-face residues. To examine whether the data support two different β-hairpin conformations, we divided the observed NOEs into native and non-native sets, and performed two separate simulated annealing calculations. In these cases, no distance violations are observed. The structures calculated with nativelike NOEs coincide with the 4:4 β-hairpin schematically represented in Figure 7a, and include the typical twist of BPTI (Figure 8a). The orientation of backbone−backbone hydrogen bond atoms is correct for a 4:4 β-hairpin in all 20 best calculated structures; in at least 12 of the 20 structures, the distances attributable to backbone−backbone hydrogen bonds are present, and the residues in the turn have dihedral angles very close to the native type I β-turn (*52*). The side chains of Y23−X30, Y21−T32, and I19−V34 interact on one side of the hairpin while the side chains of N24−L29, F22−Q31, R20−F33, and I18−Y35 residues lie on the other (Figure 8b). The structures calculated with non-native NOEs are not as well-defined because the NOEs are smaller and weaker. The orientation of backbone−backbone hydrogen bond atoms is correct for a 3:5 β-hairpin in the 20 best structures. However, distances expected for backbone−backbone hydrogen bonds in the non-native case are not observed, and the residues in the turn do not have dihedral angles corresponding to any standard turn type (*52*). The side chains of Y23−L29, Y21−Q31, I19−F33, and R17−Y35 interact on one side of the hairpin, while the side chains of F22−X30, R20−T32, and I18−V34 residues lie on the other (Figure 8c). Note that the opposite strands in the 4:4 and 3:5 β-hairpins are out of register by one residue (compare Figure 7a with 7b).

Third, De Alba et al. (*9*, *11*, *12*) have reported an equilibrium between 4:4 and 3:5 β-hairpins in a study of

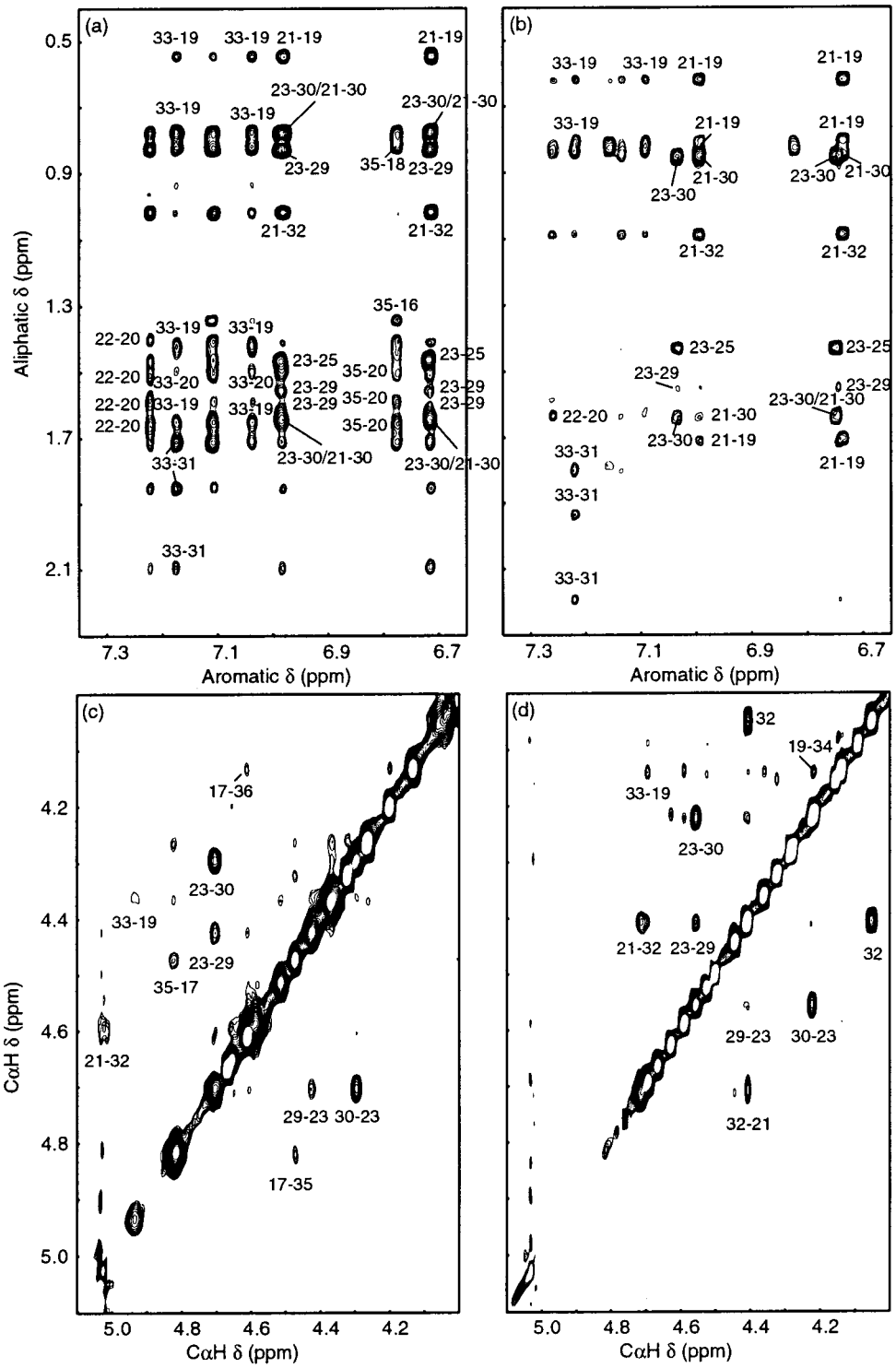

FIGURE 6: NOESY spectrum in ^2H_2O at 3 °C and pH 4.5, taken at 800 MHz, of the aromatic−aliphatic region of (a) oxidized core module and (b) reduced core module, and of the CαH−CαH region of (c) oxidized core module and (d) reduced core module.

the conformational preferences of peptides designed to fold into β-hairpins. Also, it is known from statistical studies that the first residue in a putative turn has a significant effect: thus, alanine at position 25 (from A-K-D-G) in a 4:4 β-hairpin prefers the α_R conformational space in a Ramachandran map, while asparagine at position 24 has a high tendency to populate the β region of the Ramachandran map and thus to stabilize a 3:5 β-hairpin (from N-A-K-D-G) (*51*, *52*). Among the structures that we calculate for oxidized core module with non-native NOEs, 14 of the 20 have N24 in the β region. De Alba et al. (*12*) observed that in a peptide with turn sequence N-P-D-G, which samples both 4:4 and 3:5 β-hairpins, replacement of N by A resulted in a decrease in the percentage of the latter.

Medium- and Long-Range NOEs Are Weaker for the Reduced Core Module. Reduced core module NOEs are similarly consistent with a rapid equilibrium between 4:4 β-hairpins and 3:5 β-hairpins. However, NOEs for reduced are clearly fewer and weaker than for oxidized; e.g., compare the aromatic−aliphatic region of NOESY spectra in Figure 6a,b. Figure 9 diagrams the differences in NOE strength between reduced and oxidized core modules. As the arrow

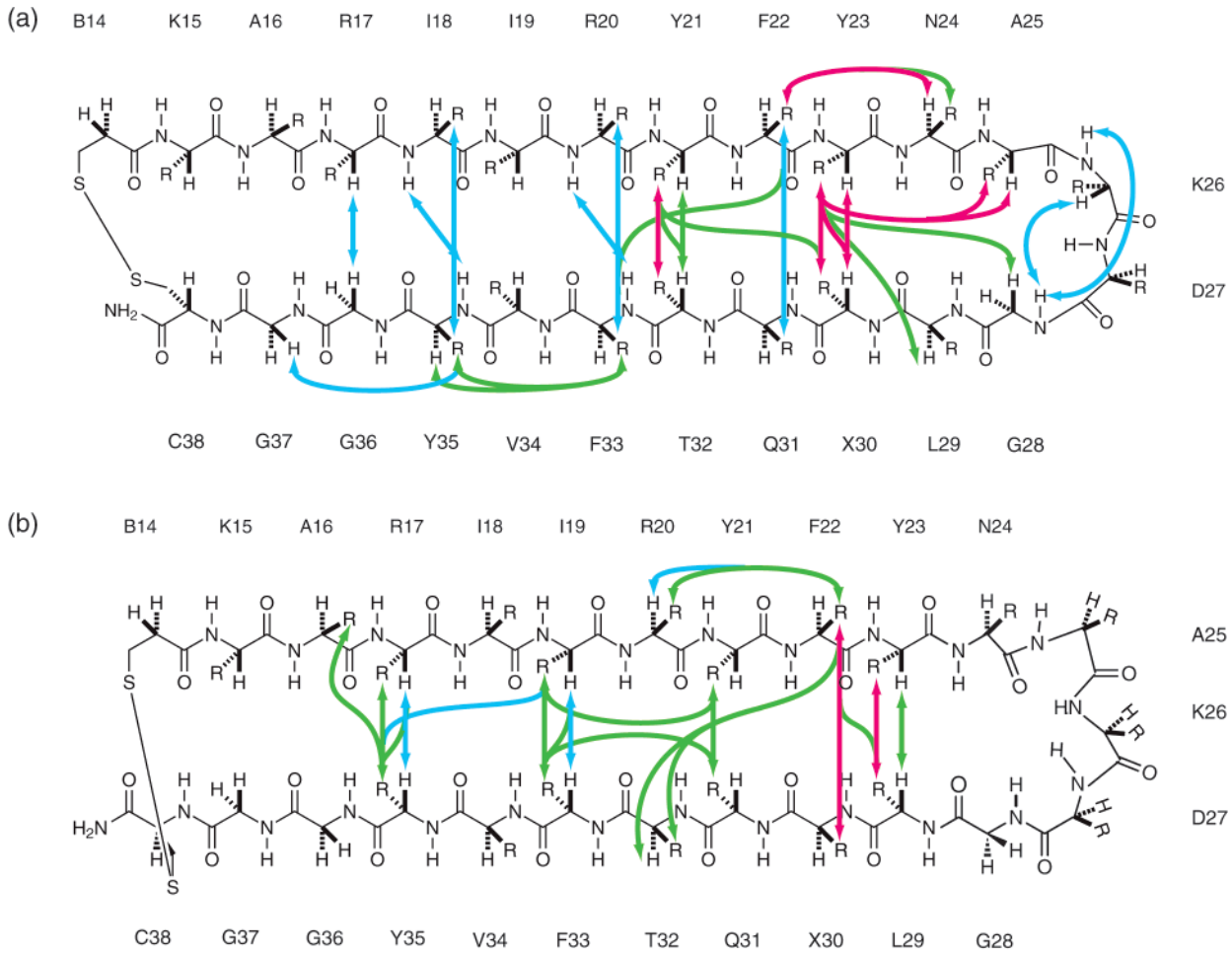

FIGURE 7: Schematic representation of long-range NOEs for the oxidized core module. NOEs observed in the oxidized module and in the 4:4 β-hairpin of native BPTI are shown in (a) as colored arrows superimposed on a 4:4 conformation. The other observed long-range NOEs in the oxidized module are consistent with a 3:5 β-hairpin, and are shown in (b) by arrows superimposed on a 3:5 β-conformation. The color of the arrow indicates NOE strength: strong ≡ red; medium ≡ green; weak ≡ blue. To reduce visual clutter, only long-range aromatic−aliphatic, CαH−CαH, and NH−CαH NOEs are included. Long-range NOEs are available in tabulated form in the Supporting Information.

pattern in Figure 9 shows, the NOEs either are observed only for oxidized, or are stronger in oxidized (e.g., the side-chain−side-chain NOEs between Y21−X30, Y21−T32, and Y23−X30), or are equally intense in both. These patterns indicate that although similar interactions may occur in the reduced core module, they are present a much smaller fraction of the time, probably due to a higher population of more flexible extended conformations.

Amide Temperature Coefficients. Andersen et al. (*55*) suggest that peptides which form ordered structure in aqueous media become increasingly disordered upon warming, and display a correlation between $\Delta\delta/\Delta T$, the amide temperature coefficient, and NH CSD, the NH chemical shift deviation from random coil calculated at the lowest temperature. The correlation coefficient for the plot of $\Delta\delta/\Delta T$ versus NH CSD is reasonable for both of our peptides: 0.75 for oxidized core module and 0.87 for reduced core module (Figure 10). The range of NH CSD at the lowest temperature is broader for the oxidized core module (+0.55 to −0.45) than for the reduced control (+0.3 to −0.5), indicating that the population of folded conformers in the oxidized core module is greater than in the reduced. The slope of the $\Delta\delta/\Delta T$ versus NH CSD correlation is steeper for reduced core module (−11.0) than for oxidized core module (−5.6), denoting greater thermal lability of folded conformers in the reduced peptide. Both peptides display reasonable correlations of $\Delta\delta/\Delta T$ versus NH CSD, leading us to conclude that there are some structured conformers at low temperature which become increasingly disordered upon warming.

Hydrogen Isotope Exchange Rates. Peptide NH exchange rates are in Table 2. Protection factors are the ratio of the experimental rate constant to the exchange rate constant calculated for unstructured peptides (*56*). While all protection factors are small (≤4.3), the high reproducibility for residues 16, 17, 26−31, and 33−36, and the fact that they vary, suggests that the differences between oxidized and reduced for 18−23 are significant. A clear increase in protection factors in oxidized versus reduced is observed for R20 (2.9 versus 1.6), Y21 (4.3 versus 2.7), and F22 (3.1 versus 2.5) (Figure 11). In native BPTI, R20, Y21, F22, and Y23 NHs are the slowest to exchange, and in $[14-38]_{Abu}$, Y21 and F22 are the slowest to exchange. In the native protein, R20, Y21, and F22 NHs are H-bonded to backbone oxygens in the middle of the antiparallel β-sheet, while Y23 NH is H-bonded to the buried side-chain carbonyl of N43. Thus, the protection factors in the oxidized core module qualitatively mirror the situation in the wild-type protein and the partially folded analogue $[14-38]_{Abu}$.

Comparison of Oxidized Core Module to Other BPTI Variants. Our laboratories have carried out extensive studies

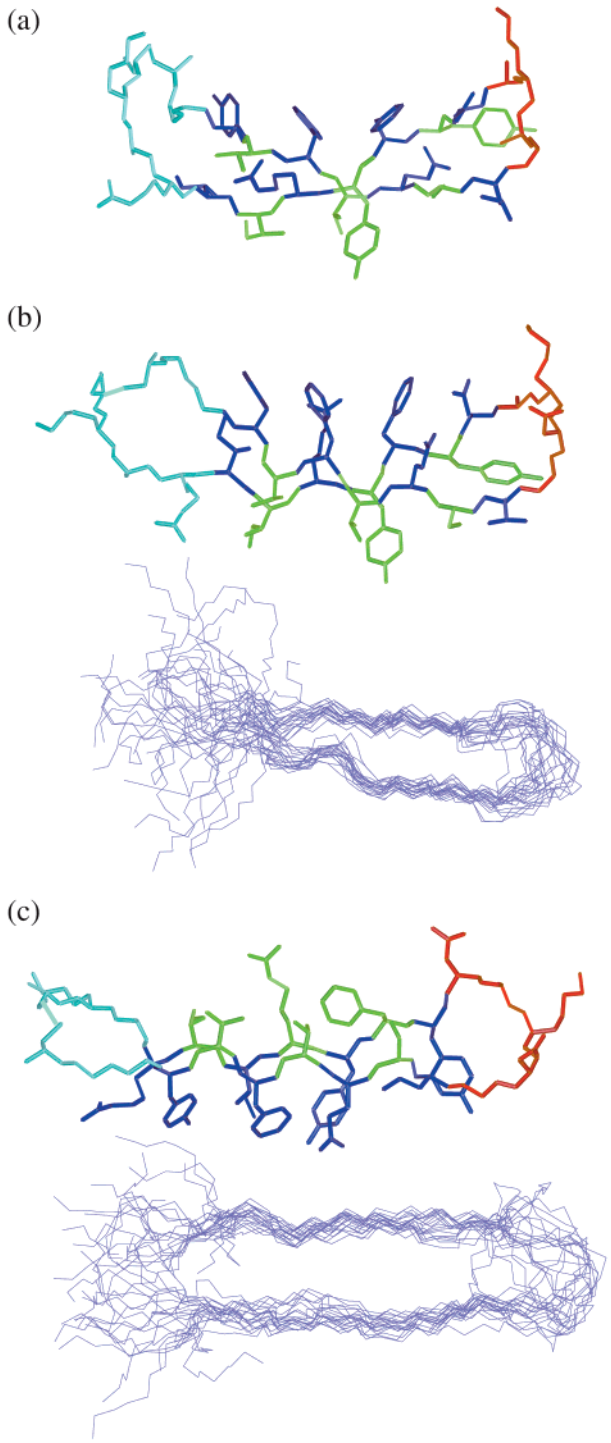

FIGURE 8: Structure of residues 14 through 38 in (a) native BPTI, based on the unique X-ray crystal structure, (b) oxidized core module, based on simulated annealing using the native NOE set, and (c) oxidized core module, based on simulated annealing using the non-native NOE set. For each of (b) and (c), the upper picture is the minimized average structure, and the lower is the superposition of the backbone atoms of the best 20 calculated structures. In the calculations, the root-mean-square (rms) deviation for backbone atoms for the native NOE set is 2.2 (residues 14−38) or 1.2 (residues 18−35) or 0.9 (residues 18−24 and 16−35). For the non-native NOE set, these values are 2.3 (residues 14−38) or 1.5 (residues 18−35) or 1.1 (residues 18−24 and 16−35). The figure was prepared with the program MOLMOL (*59*).

to characterize two BPTI variants, $[14-38]_{Abu}$ (*3*) and $[R]_{Abu}$ (*2*), which are useful models for the ensemble of transient intermediates formed during the first 10−20 ms of the protein folding process. $[14-38]_{Abu}$ with a single disulfide bond between C14 and C38, and the four remaining cysteine residues replaced by α-amino-*n*-butyric acid residues (X in Figure 1), is a model for a partially folded intermediate. At pH 4.5, $[14-38]_{Abu}$ exists as an ensemble of conformations all of which have the 18−24 and 29−35 antiparallel *β*-sheet of native BPTI essentially intact, while in the rest of the molecule, residues fluctuate between local and disordered conformations. The BPTI analogue $[R]_{Abu}$, with all six cysteines replaced by α-amino-*n*-butyric acid, is not a random coil, but rather exhibits extensive nonrandom structure reported by numerous non-native, backbone−backbone and side-chain−side-chain NOEs which involve residues that in native BPTI form the core elements. The NMR-detected structure of residues 14−38 in $[14-38]_{Abu}$ is based on native long-range NOEs, whereas that in $[R]_{Abu}$ is based on non-native short-range NOEs.

Oxidized core module exhibits NOEs comparable to those diagnostic of structure in both $[14-38]_{Abu}$ and $[R]_{Abu}$. The nativelike NOEs shown in Figure 7a are all present in spectra of $[14-38]_{Abu}$, and all of the non-native, *i*,*i*+2 backbone−backbone and side-chain−side-chain NOEs shown in Figure 7b are also present in spectra of $[R]_{Abu}$. Non-native cross-strand NOEs consistent with a 3:5 *β*-hairpin shown in Figure 7b are not observed in either $[14-38]_{Abu}$ or $[R]_{Abu}$. From these data, we conclude that the oxidized core module samples nativelike partially folded conformations, but to a lesser extent than $[14-38]_{Abu}$. Long-range NOEs indicate that, as expected, the oxidized core module is more folded than the full-length $[R]_{Abu}$, which lacks the disulfide cross-link.

Peptide Fragments from Other Proteins. Peptides with sequences from protein GB1, protein LB1, and ubiquitin have been characterized by several research teams with the idea of identifying subdomains that favor nativelike structure. In all three proteins, an *N*-terminal *β*-hairpin is connected by an α-helix to two strands of *β*-sheet at the *C*-terminus; in GB1 and LB1, the *C*-terminal strands are a hairpin, but in ubiquitin, the third and fourth *C*-terminal *β*-strands are connected by a long insertion. The conformational preferences of fragments comprised of various secondary structural elements have been reported for these proteins. For GB1, a peptide corresponding to the *C*-terminal *β*-hairpin forms a well-populated nativelike structure in aqueous solution (*17*), while one corresponding to the *N*-terminal hairpin is basically flexible in aqueous media while a set of transient nativelike *β*-hairpins are formed in 30% TFE (*16*). Further, a GB1-derived peptide with the sequence of the helix shows a low but recognizable tendency to nativelike helix in aqueous media, and a high population of helical structure in 30% TFE (*57*, *58*). For LB1, peptides corresponding to either *β*-hairpin fail to show clear preference for nativelike conformation in water, and their conformational state in TFE is uncertain as both aggregate (*20*). An LB1-derived peptide corresponding to the α-helix aggregates slightly in aqueous media, but it shows nativelike structure in 30% TFE (*20*). For ubiquitin, peptides corresponding to the hairpin plus the helix in 30% or 60% MeOH (*15*), or to the *N*-terminal *β*-hairpin in aqueous solution (*21*), favor nativelike structure.

Since our strategy for design and construction of protein core modules is based on core elements derived from hydrogen exchange analysis, it is of interest to compare the

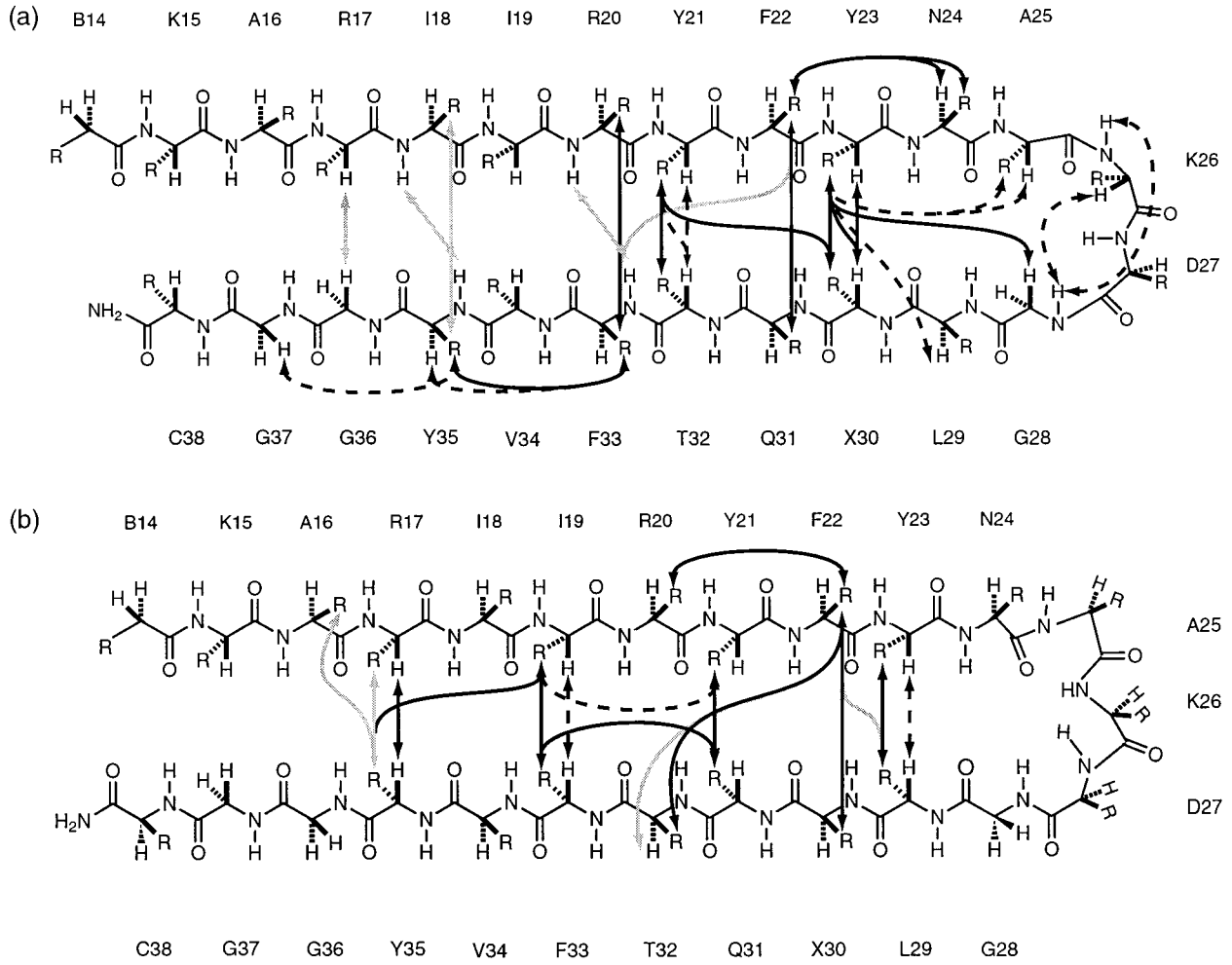

FIGURE 9: Diagram illustrating the differences in NOEs for oxidized versus reduced core modules. NOEs consistent with the native 4:4 β-hairpin are shown in (a); those consistent with a 3:5 β-hairpin are shown in (b). NOEs observed in oxidized but not in the reduced core module are gray arrows; NOEs stronger in the oxidized module are solid arrows; and NOEs of equal intensity in both peptides are dashed arrows.

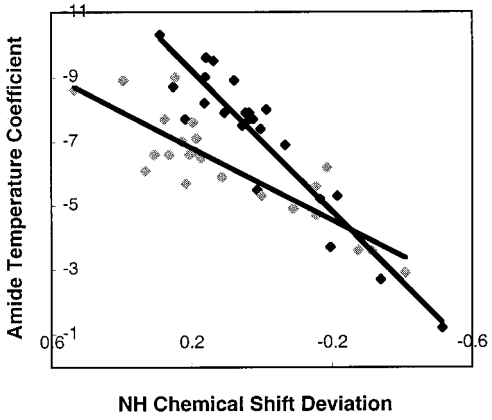

FIGURE 10: Correlation between the NH temperature gradient ($\Delta\delta/\Delta T$ in ppb/°C) over the range 3−35 °C, and the NH shift deviation (ppm) from random coil at 3 °C for oxidized core module (gray) and reduced core module (black).

hydrogen exchange cores of protein GB1, protein LB1, and ubiquitin with their respective fragment conformations. Unfortunately, none of the aforementioned proteins have been studied sufficiently for native-state exchange to allow clear identification of their core elements. The available exchange data have been summarized earlier (ref *1*; see Figure 3C in that review for proteins GB1 and LB1, and Figure 3D therein for ubiquitin). As we have discussed (*1*), in the pulsed exchange or competition experiments, rates of protein GB1 and LB1 are spread out well enough to identify NHs that are first protected, but in exchange experiments from the native state, there are too many NHs that exchange slowly under the conditions of the experiment to allow unambiguous identification of the slowest among them. In such a situation, we find that most often the secondary structural elements with the longest runs of very slowly exchanging amides are those that turn out to be in the slow exchange core. In GB1, β4 and α have the largest number of slowest exchanging NHs, and in a folding competition experiment, residues in β4 and α are protected first. In LB1, β1 and α have the largest number of slowest exchanging NHs, and in a folding competition experiment, β1 and α have the highest protection. In ubiquitin, exchange rates are not well resolved under the experimental conditions, and neither a slowest exchanging group nor a first protected group is distinguishable. However, the consecutive runs of slowest exchanging and first protected in β1 and α1 suggest that these elements are the central core of ubiquitin. In summary, although peptides of LB1 are difficult to analyze because of their propensity to aggregate, peptides of GB1 and ubiquitin that show nativelike structure are composed of sequences consistent with core elements. This suggests a reason for

Table 2: Hydrogen Exchange Rate Constants for Oxidized Core Module at 6 °C and pH 4.15 and for Reduced Core Module at 6 °C and pH 4.4

residue	oxidized module k_{obs} (min^{-1})	oxidized module K_{cx} (min^{-1})[a]	reduced module k_{obs} (min^{-1})	reduced module K_{cx} (min^{-1})[a]
Lys 15[b]	1.9×10^{-1}		1.5×10^{-1}	
Ala 16	1.1×10^{-1}	1.2×10^{-1}	1.7×10^{-1}	1.9×10^{-1}
Arg 17	6.5×10^{-2}	1.1×10^{-1}	9.4×10^{-2}	1.7×10^{-1}
Ile 18	1.3×10^{-2}	2.7×10^{-2}	3.6×10^{-2}	4.5×10^{-2}
Ile 19	6.0×10^{-3}	9.8×10^{-3}	1.3×10^{-2}	1.6×10^{-2}
Arg 20	2.2×10^{-2}	6.3×10^{-2}	6.3×10^{-2}	1.0×10^{-1}
Tyr 21	1.8×10^{-2}	7.9×10^{-2}	4.8×10^{-2}	1.3×10^{-1}
Phe 22	1.8×10^{-2}	5.7×10^{-2}	3.8×10^{-2}	9.4×10^{-2}
Tyr 23	5.1×10^{-2}	5.5×10^{-2}	5.3×10^{-2}	9.0×10^{-2}
Asn 24[c]	*c*	3.1×10^{-1}	*c*	5.1×10^{-1}
Ala 25[d]	*d*	1.8×10^{-1}	*d*	3.0×10^{-1}
Lys 26	1.3×10^{-1}	8.1×10^{-2}	2.2×10^{-1}	1.3×10^{-1}
Asp 27	1.0×10^{-1}	6.0×10^{-2}	1.4×10^{-1}	9.7×10^{-2}
Gly 28	3.5×10^{-2}	1.1×10^{-1}	5.7×10^{-2}	1.8×10^{-1}
Leu 29	1.27×10^{-2}	3.5×10^{-2}	2.0×10^{-2}	5.7×10^{-2}
Abu 30[e]	1.0×10^{-2}	1.1×10^{-2}	1.6×10^{-2}	1.8×10^{-2}
Gln 31[e]	1.9×10^{-2}	7.4×10^{-2}	3.4×10^{-2}	1.2×10^{-1}
Thr 32[c]	*c*	1.2×10^{-1}	*c*	2.0×10^{-1}
Phe 33	2.5×10^{-2}	8.1×10^{-2}	4.0×10^{-2}	1.3×10^{-1}
Val 34	9.3×10^{-3}	2.0×10^{-2}	1.9×10^{-2}	3.3×10^{-2}
Tyr 35	2.0×10^{-2}	3.5×10^{-2}	3.5×10^{-2}	5.7×10^{-2}
Gly 36	1.1×10^{-1}	1.8×10^{-1}	1.9×10^{-1}	3.0×10^{-1}
Gly 37[d]	*d*	2.4×10^{-1}	1.5×10^{-1}	4.0×10^{-1}
Cys 38[d]	*d*	4.7×10^{-1}	8.0×10^{-1}	9.0×10^{-1}

[a] Intrinsic rate constants at 6 °C were calculated by the method of Bai (*56*) using E_a of 17 kcal/mol and pD_{corr} of 4.55 for the oxidized core module and pD_{corr} of 4.8 for the reduced core module. [b] k_{cx} has not been calculated for K15, because the assumption that Mpa behaves as a Cys does not provide reliable results. [c] Intrinsic rate constants for residues N24 and T32 could not be calculated due to chemical shift overlap. [d] Rates for A25, G37, and C38 could not be measured because they exchange too rapidly. [e] The intrinsic rate constants for residues X30 and Q31 have been calculated assuming that X behaves as a valine.

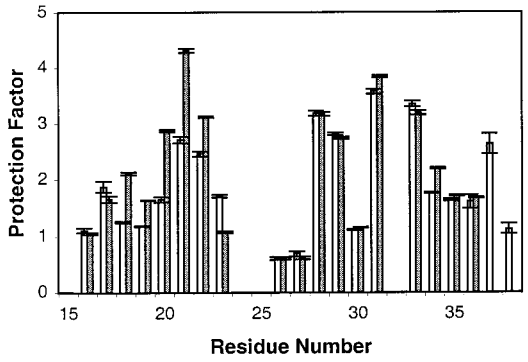

FIGURE 11: Amide NH exchange rates are expressed as protection factor of oxidized core module (filled bars) and reduced core module (open bars). Exchange rate constants and computed rate constants for an unstructured peptide are given in Table 2. Error bars correspond to the standard deviation of the nonlinear least-squares fit of the exponential rate equation to the experimental data.

why protein fragments are sometimes nativelike and sometimes are not: if the peptide consists of core elements, it seems more likely to favor native structure.

CONCLUSIONS

NMR data obtained for the designed oxidized and reduced core modules adapted from BPTI demonstrate that the ensemble of conformations sampled by the oxidized core module populates nativelike core structure a significant fraction of the time. This reinforces our conclusion from earlier experimental work and a literature review that peptides corresponding to the core elements favor nativelike structure, and suggests that the core elements determine the basic fold of the protein.

ACKNOWLEDGMENT

We are grateful to Dr. Elisar Barbar for helpful discussions and to Dr. John Battiste for help in the structure calculations. NMR experiments were performed at the University of Minnesota High Field NMR Laboratory. Workstation use was supported in part by the University of Minnesota Supercomputing Institute.

SUPPORTING INFORMATION AVAILABLE

Tables of ^{1}H NMR assignments for oxidized and reduced core modules in aqueous solution at 3 °C and pH 4.5. Tables of the sequential NOEs as well as the long-range aromatic−aliphatic NOEs for oxidized and reduced core modules in aqueous solution at 3 °C and pH 4.5. Comparison of the proton and TOCSY NMR spectra between the oxidized peptide with alanine at position 27 and the corresponding peptide with aspartic acid at position 27 (15 pages). This material is available free of charge via the Internet at http://pubs.acs.org.

REFERENCES

1. Li, R., and Woodward, C. (1999) *Protein Sci. 8*, 1571−1590.
2. Pan, H., Barbar, E., Barany, G., and Woodward, C. (1995) *Biochemistry 34*, 13974−13981.
3. Barbar, E., Barany, G., and Woodward, C. (1995) *Biochemistry 34*, 11423−11434.
4. Barbar, E. (1999) *Biopolymers 51*, 191−207.
5. Blanco, F., Ramírez-Alvarado, M., and Serrano, L. (1998) *Curr. Opin. Struct. Biol. 8*, 107−111.
6. Gellman, S. H. (1998) *Curr. Opin. Chem. Biol. 2*, 717−725.
7. Blanco, F. J., Jiménez, M. A., Herranz, J., Rico, M., Santoro, J., and Nieto, J. L. (1993) *J. Am. Chem. Soc. 115*, 5887−5888.
8. Ramírez-Alvarado, M., Blanco, F. J., and Serrano, L. (1996) *Nat. Struct. Biol. 3*, 604−612.
9. De Alba, E., Jiménez, M. A., Rico, M., and Nieto, J. L. (1996) *Folding Des. 1*, 133−144.
10. Ramírez-Alvarado, M., Blanco, F. J., Niemann, H., and Serrano, L. (1997) *J. Mol. Biol. 273*, 898−912.
11. De Alba, E., Rico, M., and Jiménez, M. A. (1997) *Protein Sci. 6*, 2548−2560.
12. De Alba, E., Jiménez, M. A., and Rico, M. (1997) *J. Am. Chem. Soc. 119*, 175−183.
13. Stanger, H. E., and Gellman, S. H. (1998) *J. Am. Chem. Soc. 120*, 4236−4237.
14. Maynard, A. J., Sharman, G. J., and Searle, M. S. (1998) *J. Am. Chem. Soc. 120*, 1996−2007.
15. Cox, J. P. L., Evans, P. A., Packman, L. C., Williams, D. H., and Woolfson, D. N. (1993) *J. Mol. Biol. 234*, 483−492.
16. Blanco, F. J., Jiménez, M. A., Pineda, A., Rico, M., Santoro, J., and Nieto, J. L. (1994) *Biochemistry 33*, 6004−6014.
17. Blanco, F. J., Rivas, G., and Serrano, L. (1994) *Nat. Struct. Biol. 1*, 584−590.
18. Searle, M. S., Williams, D. H., and Packman, L. C. (1995) *Nat. Struct. Biol. 2*, 999−1006.
19. Haque, T. S., and Gellman, S. H. (1997) *J. Am. Chem. Soc. 119*, 2303−2304.
20. Ramírez-Alvarado, M., Serrano, L., and Blanco, F. J. (1997) *Protein Sci. 6*, 162−174.
21. Zerella, R., Evans, P. A., Ionides, J. M. C., Packman, L. C., Trotter, B. W., Mackay, J. P., and Williams, D. H. (1999) *Protein Sci. 8*, 1320−1331.

22. Barany, G., Gross, C. M., Ferrer, M., Barbar, E., Pan, H., and Woodward, C. (1996) *Techniques in Protein Chemistry VII*, pp 503−514, Academic Press, San Diego, CA.
23. Han, Y., Albericio, F., and Barany, G. (1997) *J. Org. Chem. 62*, 4307−4312.
24. Griesinger, C., Otting, G., Wüthrich, K., and Ernst, R. R. (1988) *J. Am. Chem. Soc. 110*, 7870−7872.
25. Kumar, A., Ernst, R. R., and Wüthrich, K. (1980) *Biochem. Biophys. Res. Commun. 95*, 1−6.
26. Piotto, M., Saudek, V., and Sklenár, V. (1992) *J. Biomol. NMR 2*, 661−665.
27. Delaglio, F., Grzesiek, S., Vuister, G. W., Zhu, G., Pfeifer, J., and Bax, A. (1995) *J. Biomol. NMR 6*, 277−293.
28. Johnson, B. A., and Blevins, R. A. (1994) *J. Biomol. NMR 4*, 603−614.
29. Brunger, A. (1992) *X-Plor (Version 3.1) Manual*, Yale University Press, New Haven, CT.
30. Wright, P. E., Dyson, J. H., and Lerner, R. A. (1988) *Biochemistry 27*, 7167−7175.
31. Dyson, J. H., and Wright, P. E. (1991) *Annu. Rev. Biophys. Biophys. Chem. 20*, 519−538.
32. Dyson, J. H., and Wright, P. E. (1993) *Curr. Opin. Struct. Biol. 3*, 60−65.
33. Mayo, K. H. (1997) *Methods Enzymol. 289*, 646−672.
34. McDonald, I., Naylor, D., Jones, D., and Thornton, J. (1993) *HBPLUS*, Department of Biochemistry and Molecular Biology, University College London.
35. Laskowski, R. A., MacArthur, M. W., Moss, D. S., and Thornton, J. M. (1993) *J. Appl. Crystallogr. 26*, 283−291.
36. McDonnell, J. M., Fusham, D., Cahill, S. M., Sutton, B. J., and Cowburn, D. (1997) *J. Am. Chem. Soc. 119*, 5321−5328.
37. Syud, F. A., Espinosa, J. F., and Gellman, S. H. (1999) *J. Am. Chem. Soc. 121*, 11577−11578.
38. Hutchinson, E. G., and Thornton, J. M. (1994) *Protein Sci. 3*, 2207−2216.
39. Woody, R. W. (1978) *Biopolymers 17*, 1451−1467.
40. Oas, T. G., and Kim, P. S. (1988) *Nature 336*, 42−48.
41. Goodman, E. M., and Kim, P. S. (1989) *Biochemistry 28*, 4343−4347.
42. Staley, J. P., and Kim, P. S. (1990) *Nature 344*, 685−688.
43. Goodman, E. M., and Kim, P. S. (1990) *Curr. Res. Protein Chem.*, 301−308.
44. Wüthrich, K. (1986) *NMR of Proteins and Nucleic Acids*, John Wiley, New York.
45. Reymond, M. T., Merutka, G., Dyson, J. H., and Wright, P. E. (1997) *Protein Sci. 6*, 706−716.
46. Padmanabhan, S., Jiménez, M. A., and Rico, M. (1999) *Protein Sci. 8*, 1675−1688.
47. Wishart, D. S., Bigam, C. G., Holm, A., Hodges, R. S., and Sykes, B. D. (1995) *J. Biomol. NMR 5*, 67−81.
48. Merutka, G., Dyson, J. H., and Wright, P. E. (1995) *J. Biomol. NMR 5*, 14−24.
49. Ösapay, K., and Case, D. A. (1994) *J. Biomol. NMR 4*, 215−230.
50. Wagner, G., and Wüthrich, K. (1982) *J. Mol. Biol. 155*, 347−366.
51. Sibanda, B. L., Blundell, T. L., and Thornton, J. M. (1989) *J. Mol. Biol. 206*, 759−777.
52. Sibanda, B. L., and Thornton, J. M. (1991) *Methods Enzymol. 202*, 59−82.
53. Ramírez-Alvarado, M., Kortemme, T., Blanco, F. J., and Serrano, L. (1999) *Bioorg. Med. Chem. 7*, 93−103.
54. Lacroix, E., Kortemme, T., López de la Paz, M., and Serrano, L. (1999) *Curr. Opin. Struct. Biol. 9*, 487−493.
55. Andersen, N. H., Neidigh, J. W., Harris, S. M., Lee, G. M., Liu, Z., and Tong, H. (1997) *J. Am. Chem. Soc. 119*, 8547−8561.
56. Bai, Y., Milne, J. S., Mayne, L., and Englander, S. W. (1993) *Proteins: Struct., Funct., Genet. 17*, 75−86.
57. Blanco, F. J., and Serrano, L. (1995) *Eur. J. Biochem. 230*, 634−649.
58. Blanco, F. J., Ortiz, A. R., and Serrano, L. (1997) *Folding Des. 2*, 123−133.
59. Koradi, R., Billeter, M., and Wüthrich, K. (1996) *J. Mol. Graphics 14*, 51−55.
60. (a) Carulla, N., Woodward, C., and Barany, G. (1999) Fortieth Experimental Nuclear Magnetic Resonance Conference, Orlando, FL, February 28−March 5, 1999. (b) Sixteenth American Peptide Symposium, Minneapolis, MN, June 26−July 1, 1999; Carulla, N., Woodward, C., and Barany, G. (2000) in *Peptides for the New Millennium: Proceedings of the 16th American Peptide Symposium* (Fields, G. B., Tam, J. P., and Barany, G., Eds.) pp 36−37, Kluwer Academic Publishers, Dordrecht, The Netherlands. (c) Sixth International Symposium on Solid-Phase Synthesis & Combinatorial Chemical Libraries, York, England, August 31−September 4, 1999; Carulla, N., Woodward, C., and Barany, G. (2000) in *Innovation and Perspectives in Solid-Phase Synthesis & Combinatorial Chemical Libraries, 2000, Collected Papers, Sixth International Symposium* (Epton, R., Ed.) Mayflower Scientific, Kingswinford, U.K. (in press).

BI992927L